AIAA JOURNAL
Vol. 39, No. 2, February 2001

Simulation of Flow About Flapping Airfoils Using Finite Element Incompressible Flow Solver

Ravi Ramamurti* and William Sandberg†
U.S. Naval Research Laboratory, Washington, D.C. 20375

A finite element flow solver based on unstructured grids is employed for studying the unsteady flow past oscillating airfoils. The viscous flow past a NACA0012 airfoil at various pitching frequencies is simulated. The variation of the force coefficient with reduced frequency is compared to experimental and other numerical studies. The effect of variation of the amplitude of the pitching motion on the force coefficient shows that the critical parameter for thrust generation is not the reduced frequency but the Strouhal number based on the maximum excursion of the trailing edge. The flow about the airfoil in a combined pitching and heaving motion, a mode found in many insects, is also simulated. The effects of varying the phase angle between the pitch and the heave motions is studied. The thrust coefficient was compared with experimental studies and good agreement is obtained. It is found that the maximum thrust coefficient is obtained for when the pitch motion leads the heave motion by 120 deg and maximum propulsive efficiency occurs at a phase angle of 90 deg.

Nomenclature

A	=	amplitude of heave motion
C_d	=	coefficient of drag, $F_x/q_\infty c$
C_l	=	coefficient of lift, $F_y/q_\infty c$
C_m	=	coefficient of moment, $M/q_\infty c^2$
C_p	=	coefficient of power, $-C_l\dot{y} - C_m\dot{\theta}$
C_T	=	coefficient of thrust, $T/q_\infty c$
c	=	chord length
F	=	force
f	=	frequency of oscillation, Hz
f^*	=	nondimensional frequency, $fc/2U_\infty$
h	=	wake width
k	=	reduced frequency, $2\pi fc/2U_\infty$
M	=	moment about pivot point
q_∞	=	freestream dynamic pressure, $1/2\rho_\infty U_\infty^2$
r	=	distance from center of rotation
Sr	=	Strouhal number, fh/U_∞
T	=	thrust, $-F_x$
t	=	time
U_∞	=	freestream velocity
$\boldsymbol{v}$	=	flow velocity
$\boldsymbol{w}$	=	mesh velocity
x, y	=	Cartesian coordinates, nondimensionalized by chord
$\alpha(t)$	=	instantaneous angle of attack
θ	=	pitch angle
θ_0	=	amplitude of pitch motion
ρ_∞	=	freestream density
ϕ	=	phase angle between pitch and heave motions

Subscripts

p	=	pressure contribution
v	=	viscous contribution
∞	=	freestream value

Introduction

FLAPPING foil propulsion, similar to the thunniform mode (lunate-tail oscillation) of fish propulsion, has received considerable attention in the past few years as an alternative to the propeller. This mode of propulsion, which involves no body undulation, has many applications, such as submersibles propulsion, maneuvering, and flow control, which are of interest to the hydrodynamic community. The unconventional aerodynamics of flapping airfoils are of interest to the aerodynamic community for the design of micro-aerial vehicles (MAV) and the study of aircraft flutter. This mode of propulsion is also important in the area of biofluid dynamics, for the study of propulsion in insects, birds, and certain aquatic animals. Experimental work on flapping foils have been carried out by Koochesfahani[1] and Anderson.[2] Computational studies have been performed by Jones and Platzer.[3] Our computational results are compared with these earlier works. Recently, Tuncer and Platzer[4] have studied numerically the viscous effects of the thrust and propulsive efficiency of single flapping airfoil at Reynolds number $Re = 3 \times 10^6$. In this paper, we investigate the thrust generation mechanism of a flapping foil undergoing pitching and pitching and heaving motions at very low Reynolds numbers.

In this study, a finite element based incompressible flow solver based on simple, low-order elements is employed. The simple elements enable the flow solver to be as fast as possible, reducing the overhead in building element matrices, residual vectors, etc. The governing equations are written in arbitrary Lagrangian Eulerian (ALE) form, which enables simulation of flow with moving bodies. For high Reynolds number flow cases, the mesh requirement is met by employing arbitrary semistructured grids close to wetted surfaces and wakes. The details of the flow solver, the rigid-body motion, and adaptive remeshing are given by Ramamurti et al.[5] and are summarized next.

Incompressible Flow Solver

The governing equations employed are the incompressible Navier–Stokes equations in ALE formulation. They are written as

$$\frac{D\boldsymbol{v}}{Dt} + \boldsymbol{v}_a \cdot \nabla \boldsymbol{v} + \nabla p = \nabla \cdot \sigma \tag{1a}$$

$$\frac{D\boldsymbol{v}}{Dt} = \frac{\partial \boldsymbol{v}}{\partial t} + \boldsymbol{w} \cdot \nabla \boldsymbol{v} \tag{1b}$$

$$\nabla \cdot \boldsymbol{v} = 0 \tag{2}$$

Here p denotes the pressure, $\boldsymbol{v}_a = \boldsymbol{v} - \boldsymbol{w}$, the advective velocity vector (flow velocity $\boldsymbol{v}$ minus mesh velocity $\boldsymbol{w}$), and the material derivative is with respect to the mesh velocity $\boldsymbol{w}$. Both the pressure p and the stress tensor σ have been normalized by the (constant) density ρ and are discretized in time using an implicit time-stepping procedure. It is important for the flow solver to be able to capture the unsteadiness of a flowfield. The present flow solver is built as time

Presented as Paper 99-0652 at the AIAA 37th Aerospace Sciences Meeting, Reno, NV, 11–14 January 1999; received 26 February 1999; revision received 6 June 1999; accepted for publication 21 June 2000.

*Aerospace Engineer, Code 6410, Laboratory for Computational Physics and Fluid Dynamics. Senior Member AIAA.

†Deputy Director, Code 6401, Laboratory for Computational Physics and Fluid Dynamics.

accurate from the onset, allowing local time stepping as an option. The resulting expressions are subsequently discretized in space using a Galerkin procedure with linear tetrahedral elements. To be as fast as possible, the overhead in building element matrices, residual vectors, etc., should be kept to a minimum. This requirement is met by employing simple, low-order elements that have all of the variables (u, v, w, and p) at the same location. The resulting matrix systems are solved iteratively using a preconditioned gradient algorithm (PCG), as described by Martin and Löhner.[6] The flow solver has been successfully evaluated for both two-dimensional and three-dimensional laminar and turbulent flow problems by Ramamurti and Löhner[7] and Ramamurti et al.[8]

Rigid-Body Motion and Adaptive Remeshing

To couple fully the motion of rigid bodies with the hydrodynamic or aerodynamic forces exerted on them, consistent rigid-body motion integrators must be developed. The governing equations of motion for rigid bodies are well known and are given by Meirovitch[9] and, for multiple bodies in relative motion, by Sandberg.[10] In the present work, the pressure distribution on the surface is integrated to compute forces and moments at each time step, and the equations of motion are advanced in time to produce self-consistent trajectories. A more detailed description of the equations and the incorporation of the rigid-body motion in the numerical scheme for solving the fluid flow are described by Ramamurti et al.[5]

To carry out computations of the flow about oscillating and deforming geometries, one needs to describe grid motion on a moving surface and couple the moving surface grid to the volume grid. The volume grid in the proximity of the moving surface is then remeshed, to eliminate badly distorted elements. A representative application requiring these gridding capabilities is the computation of the flow about pitching and heaving airfoils and the computation of vorticity shedding from the edges of oscillating foils. It is also essential for computing the flow past objects that are both accelerating and deforming. In deformations, the surface motion may be severe, leading, in the absence of remeshing, to distorted elements that in turn lead to poor numerical results. If the bodies in the flowfield undergo arbitrary movement, a fixed mesh structure will lead to badly distorted elements. This means that at least a partial regeneration of the computational domain is required. On the other hand, if the bodies move through the flowfield, the positions of relevant flow features will change. Therefore, in most of the computational domain a new mesh distribution will be required.

One approach to solve these problems is to add several layers around the moving bodies that move rigidly with the body. As the elements (or edges) move, their geometric parameters (shape-function derivatives, Jacobians, etc.) need to be recomputed at every time step. If the whole mesh is assumed to be in motion, then these geometric parameters need to be recomputed globally. To save CPU time, only a small number of elements surrounding the bodies are actually moved. The remainder of the field is then treated in the usual Eulerian frame of reference, which avoids the need to recompute geometric parameters. This may be accomplished in a variety of ways, of which the two most common are 1) identifying several layers of elements surrounding the surfaces that move and 2) moving all elements within a certain distance from the surfaces that move. Both approaches have their advantages and disadvantages and are, therefore, treated in more detail.

Layers of Moving Elements

In this case, the elements moved are obtained by starting from the moving surfaces and performing n number of passes over nearest neighbors to construct the n layers of elements that move. This procedure is extremely fast and works only with integer variables. On the other hand, for situations where the element size varies rapidly, the moving mesh region can assume bizarre shapes. This, in turn, may force many remeshings at a later stage. This type of procedure is most commonly used for Euler calculations.[11,12]

Elements Within a Distance

This second approach requires the knowledge of the distance of a point from the moving surfaces. All elements within a prescribed distance from the moving surfaces are considered as moving. Although this procedure required more CPU time when being built, it offers the advantage of a very smooth boundary of the moving mesh region. Moreover, by specifying two distances, the region close to the moving surfaces may be moved in the same way the surfaces move, whereas farther away the mesh velocity is smoothed as before. This allows the movement of Navier–Stokes-type grids that are very elongated and, hence, sensitive to any kind of distortion, as shown by Ramamurti and Löhner.[7]

Mesh Movement Algorithms

An important question from the point of view of mesh distortion and remeshing requirements is the algorithm employed to move the mesh. Assume that the mesh velocity on the moving surfaces of the computational domain is prescribed as follows:

$$\boldsymbol{w}|_{\Gamma_m} = \boldsymbol{w}_0 \tag{3}$$

At a certain distance from these moving surfaces, as well as all of the remaining surfaces, the mesh velocity vanishes:

$$\boldsymbol{w}|_{\Gamma_0} = 0 \tag{4}$$

The question now is, how to obtain a mesh velocity field $\boldsymbol{w}$ in such a way that element distortion is minimized? A number of algorithms have been proposed. They may be grouped together into the following categories: 1) prescribing the mesh velocity analytically, 2) smoothing the coordinates, and 3) smoothing the velocity field.

Prescription via Analytic Functions

In this case, the mesh velocity is prescribed to be an analytic function based on the distance from the surface. By the use of heap lists, as well as other optimal data structures, the distance from the surface may be obtained in $\mathcal{O}(N \log N)$ operations, where N is the number of grid points. Given this distance r and the point on the surface closest to it $\boldsymbol{x}|_\Gamma$, the mesh velocity is given by

$$\boldsymbol{w} = \boldsymbol{w}(\boldsymbol{x}|_\Gamma)\, f(r) \tag{5}$$

The function $f(r)$ assumes the value of unity for $r = 0$ and decays to zero as r increases. This makes the procedure somewhat restrictive for general use, particularly if several moving bodies are present in the flowfield. On the other hand, the procedure is extremely fast if the initial distance r can be employed for all times.[13]

Smoothing of the Coordinates

In this case, we start with the prescribed boundary velocities. This yields a new set of boundary coordinates at the new time step:

$$\boldsymbol{x}^{n+1}|_\Gamma = \boldsymbol{x}^n|_\Gamma + \Delta t \boldsymbol{w}|_\Gamma \tag{6}$$

The mesh is smoothed based on these new values for the coordinates of the boundary points. In most cases to date, a simple spring analogy smoother has been employed. The new values for the coordinates are obtained iteratively via a relaxation or conjugate gradient scheme.[14,15] As before, a good initial guess may be extrapolated via

$$\boldsymbol{x}_0^{n+1} = 2\boldsymbol{x}^n - \boldsymbol{x}^{n-1} \tag{7}$$

The smoothed mesh velocity is then given by

$$\boldsymbol{w} = (1/\Delta t)(\boldsymbol{x}^{n+1} - \boldsymbol{x}^n) \tag{8}$$

Most of the potential problems that may occur for this type of mesh velocity smoothing are due to initial grids that have not been smoothed. For such cases, the velocity of the moving boundaries is superposed to a fictitious mesh smoothing velocity that may be quite large during the initial stages of a run. Moreover, if spring analogy smoothers are employed, there is no guarantee that negative elements will not appear.

Smoothing of the Velocity Field

In this case, the mesh velocity is smoothed, based on the exterior boundary conditions given by Eqs. (3) and (4). The aim, as stated before, is to obtain a mesh velocity field $\boldsymbol{w}$ in such a way that element distortion is minimized.

In this study, the smoothing of the coordinates was employed for the mesh movement with a specified number of layers of elements that move rigidly with the pitching or pitching and heaving airfoil. This method was successful for the pitching airfoil cases and for the pitching and heaving airfoil case when the initial pitch angle of attack was 15 deg. This meant that the mesh around the airfoil would undergo a 30-deg rotation during a complete cycle. As the initial pitch angle of attack was increased to 30 deg, it was apparent that negative elements would appear at the edge of the layers of elements that move rigidly with the body. The reason for this is that the spring analogy that is employed does not guarantee that negative elements will not appear. Also, a closer look at the grid showed that the elements at the edge of the rigid layers were quite distorted after one cycle of oscillation. This is due to a residual mesh velocity that is present due to the nonconvergence of the mesh velocity field. This will appear whether a spring analogy is used or a Laplacian-based smoothing is used.

To recover the original mesh after one cycle of oscillation, the coordinates at the new time were obtained as a weighted average of the original grid point location at time $t = 0$ and the location of the point as if it moved rigidly with the body:

$$\boldsymbol{x}^{n+1} = \boldsymbol{x}^{0} f(r) + \boldsymbol{x}^{n+1}_{\text{rigid}}[1 - f(r)] \tag{9}$$

where the weighting function is a simple linear function based on the distance from the center of rotation r and is given by

$$\begin{aligned} f(r) &= 0 && \text{for} \quad r < r_{\min} \\ &= 1 && \text{for} \quad r > r_{\max} \\ &= \frac{(r - r_{\min})}{(r_{\max} - r_{\min})} && \text{for} \quad r_{\max} > r > r_{\min} \end{aligned} \tag{10}$$

The mesh velocity is then obtained using Eq. (8). This ensured that the original grid was recovered after one cycle of oscillation. This procedure is robust and cheap in terms of computational time, involving only one distance computation, and can be generalized for multiple moving bodies with prescribed motion by modifying the weighting function appropriately.

Discussion of Results

The configuration used for the flow simulations over the pitching, and pitching and heaving, NACA0012 airfoil is shown in Fig. 1. The heaving motion of the airfoil is referenced to the pivot point, located at x_p from the leading edge, and is given by

$$y(t) = A \sin(2\pi f t) \tag{11}$$

where A is the amplitude of the heaving motion and f is the frequency of oscillation in hertz. The pitching motion of the airfoil leads the heaving motion by a phase angle ϕ and is given by

$$\theta(t) = \theta_0 \sin(2\pi f t + \phi) \tag{12}$$

where θ_0 is the amplitude of the pitching motion. The instantaneous angle of attack $\alpha(t)$ is obtained from the fluid velocity U_∞, the heave velocity $\dot{y}(t)$, and the pitch angle $\theta(t)$. This can be written as

$$\alpha(t) = \theta(t) - \tan^{-1}[\dot{y}(t)/U_\infty] \tag{13}$$

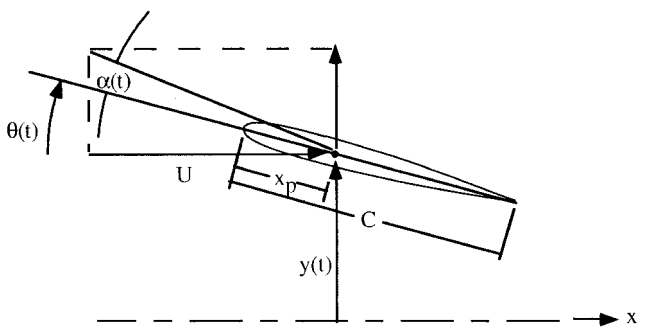

Fig. 1 Schematic of the pitching and heaving airfoil.

Pitching Airfoil

The flow solver described here is employed to compute the flow about a pitching NACA0012 airfoil. The Reynolds number based on chord was 1.2×10^4. The computational grid consisted of 10,098 points and 19,974 triangular elements. The semistructured mesh near the airfoil was constructed so that the first point is at a distance of 4×10^{-6} away from the wall, and approximately 30 points are within the boundary layer. Several laminar flow simulations were performed for a range of frequency f, between 1 and 8 Hz and a pitch amplitude of 2 deg. The force on the airfoil was computed by integrating the pressure and the viscous shear stresses on the surface. The force coefficient was then computed by normalizing the pressure and viscous components of the forces with the dynamic head of the freestream, as shown in the Nomenclature.

To assess the independence of the computed solution with grid refinement, two finer grids, consisting of 18,000 and 44,000 points, were employed for the case of $f = 5$ Hz. The effect of grid refinement on the force component in the x direction, F_x, due to pressure is shown in Fig. 2a, and the time history of the force is observed to be grid independent. The viscous shear forces showed a high-frequency oscillation in the solution with 10,000 points (Fig. 2b). These oscillations disappeared with the 18,000- and 44,000-point

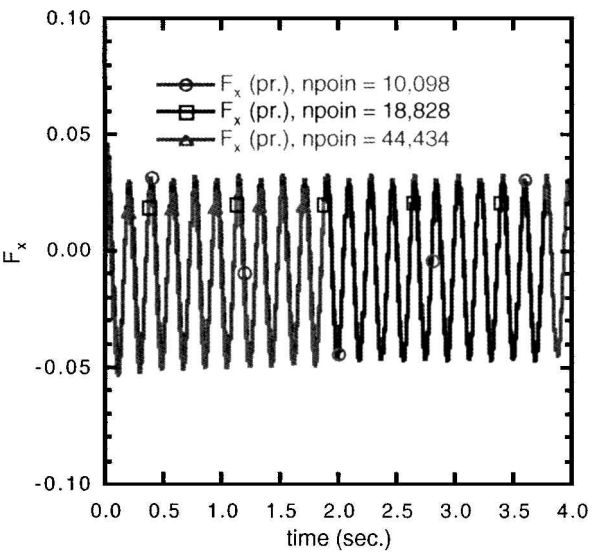

a) Pressure component

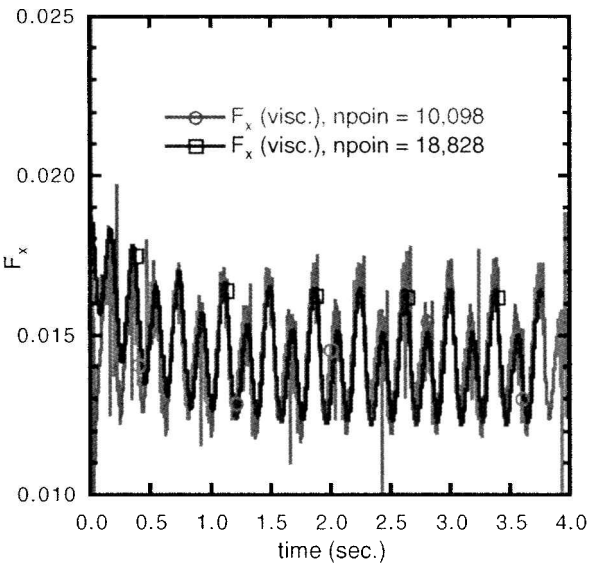

b) Viscous component

Fig. 2 Effect of grid refinement.

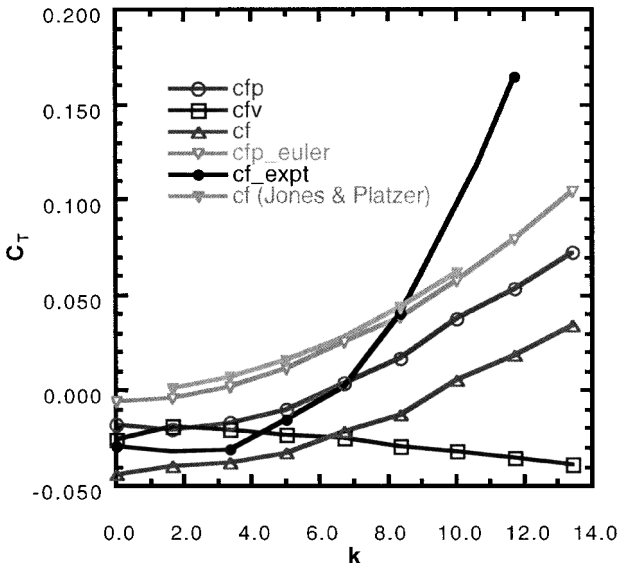

Fig. 3 Comparison of thrust coefficient.

solutions. However, the mean of the viscous forces remained almost grid independent.

The results were then compared to those from the experiments by Koochesfahani.[1] The variation of the force coefficient with reduced frequency, $k = 2\pi f C/2U_\infty$, is shown in Fig. 3. The drag coefficient C_d is computed from the sum of the force obtained by integrating the pressure F_{xp} and the viscous forces F_{xv} on the surface of the airfoil and normalizing with the freestream dynamic head. The thrust coefficient C_T is then taken to be the negative value of C_d. A negative value of the thrust coefficient indicates a drag force, whereas a positive value indicates thrust generation. The computed values underpredict the experimental values. To determine the origin of the differences, an inviscid computation was performed for these frequencies. The computed results were compared to the numerical results of Jones and Platzer,[3] and the agreement is good. From Fig. 3, it is clear that the thrust coefficient for the viscous cases is similar to that of the inviscid flow with a reduction in magnitude for all of the frequencies computed. This implies that the viscous contribution to the total force is small. Hence, the inviscid results represent an upper bound for the thrust. Therefore, the thrust calculations from the experiments are increasingly in error with increasing frequency. Similar discrepancies with this experiment have been documented by Jones and Platzer[3] and Liu and Kawachi.[16]

In the experimental investigation by Koochesfahani,[1] the drag or thrust generated by a body is computed by measuring the momentum deficit or gain downstream of the body. The flow is assumed to be parallel at the cross section where the velocities are measured and the time fluctuating quantities are small. Hence, the coefficient of thrust can be computed from the following integral:

$$T = -\int_{-\infty}^{+\infty} \rho\left[u^2(y) - U_\infty^2\right] \mathrm{d}y$$

$$= -\rho \int_{-\infty}^{+\infty} u(y)[u(y) - U_\infty] \mathrm{d}y \tag{14}$$

$$C_T = \frac{2}{c} \int_{-\infty}^{+\infty} \frac{u(y)}{U_\infty}\left[\frac{u(y)}{U_\infty} - 1\right] \mathrm{d}y \tag{15}$$

If the velocity measurements are made at a location far downstream of the airfoil where the eddies are diffused, the results will be reasonable, if the integration domain is sufficiently large. Instead, if the eddies are still coherent at the measurement plane, the assumptions will not hold. In experiments,[1] the measuring plane seems to have been placed at one chord length downstream of the trailing edge where the eddies are still present.

To further clarify the wake integration issue, the mean velocity profile in the wake was computed in the unsteady flow simulation. The velocity profile downstream of the airfoil was averaged in time, and the force coefficient was computed by integrating the resultant velocity profile. Three locations were selected at $x = 0.1$, 0.5, and 1.0 chord lengths downstream of the trailing edge of the airfoil for the integration of the velocity profile. The results showed that for a frequency $f = 5$ Hz, the force coefficient through integration at these three locations are -0.0036, -0.0117, and -0.0148, respectively. The thrust coefficient from the integration of the pressure and shear stresses on the surface of the airfoil was -0.0124. It is clear that the values from the surface integral fall between the values from the wake integrals and that the thrust coefficient from the wake integral is sensitive to the location. Thus, the computations indicate a drag force whereas the experimental value for this case is $+0.04068$. The discrepancy between the experiment and the computation may also be due to the presence of the tunnel walls in the experiment. Hence, to investigate this possibility computationally, the outer walls were placed at two chord lengths away on either side of the airfoil. The thrust coefficient from the wake profiles at the three locations for this case are $+0.00463$, -0.00655, and -0.00901, respectively. The thrust coefficient from the integration of the pressure and shear stresses on the surface of the airfoil was -0.00904. The tunnel walls, in effect, increase the thrust coefficient, but only marginally. It is not clear from Ref. 1 how far downstream the measurements were made to obtain the thrust in the experiments. Hence, we conclude that the

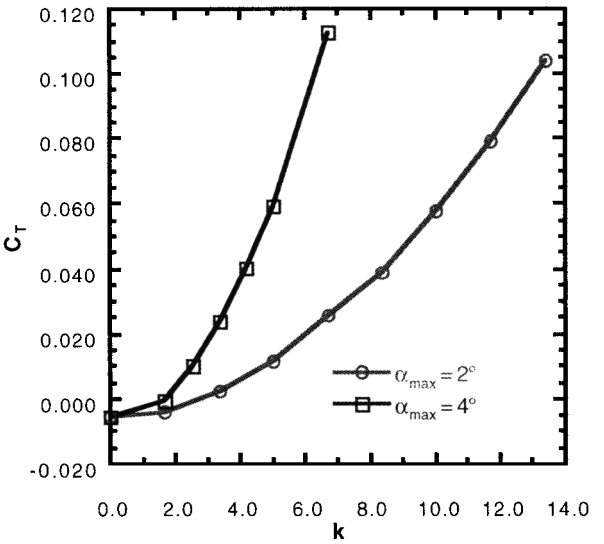

a) C_T vs reduced frequency

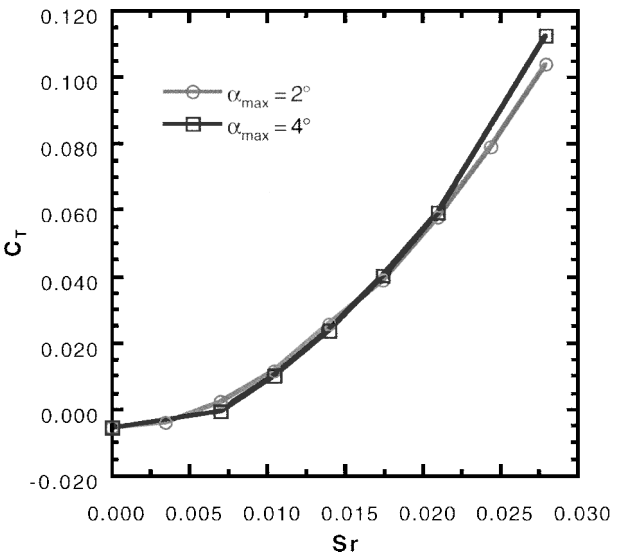

b) C_T vs Strouhal number

Fig. 4 Variation of thrust coefficient for an oscillating airfoil.

differences between the experimental data and the computations are due to the exclusion of a contribution of the fluctuating quantities and the pressure term in the experimental thrust computation at the measuring location and possibly three-dimensional effects in the tunnel, which is not in the scope of this study.

At low frequencies of oscillation, a Karman vortex street is observed downstream of the trailing edge. Here, the clockwise-rotating vortices are observed on the upper row with counterclockwise-rotating vortices on the lower row. As the frequency of oscillation is increased, the upper row of vortices are rotating counterclockwise, and the lower row rotates clockwise, as a reverse Karman vortex street. In these cases, these vortices induce a momentum gain in the vicinity of the wake centerline. It is also observed that in these cases a thrust is produced instead of drag. These wake patterns were also observed in the visualizations of Koochesfahani.[1] From Fig. 3, the reduced frequency at which there is a crossover from drag to thrust is approximately 3.35 for inviscid case and approximately 10.0 for the viscous case.

Effect of Pitch Amplitude

Next, the amplitude of the pitching oscillation was increased from 2 to 4 deg. First, an inviscid flow simulation was carried out for various frequencies for both of these amplitudes. The variation of the coefficient of thrust C_T was plotted against the reduced frequency k in Fig. 4a. The critical value of k for thrust generation seems to depend on the amplitude of oscillation. Next the variation of C_T with respect to the Strouhal number was plotted in Fig. 4b. For this purpose, the Strouhal numbers $Sr = fh/U_\infty$ was defined based on the wake width h. Because the wake width is not generally known, the maximum excursion of the trailing edge of the airfoil is taken as a close approximation because it is a physically relevant length scale in the process. It is clear from Fig. 4b that the governing parameter for the thrust coefficient is not the reduced frequency but the Strouhal number based on the trailing-edge displacement. Viscous flow simulations were also performed at various frequencies for these two amplitudes at $Re = 1.2 \times 10^4$. A similar behavior of the thrust coefficient with k and Strouhal numbers is observed and is shown in Figs. 5a and 5b, respectively. It is seen in Figs. 4b and 5b that the magnitude of the thrust coefficient is independent of the Strouhal number based on trailing-edge displacement. At $Sr = 0.028$, the results indicate that there is a dependency on the pitch amplitude. This dependency is more pronounced in the viscous case compared to the invicid case. Therefore, this dependency of the thrust coefficient variation at high Strouhal numbers and for large pitch amplitudes (>4 deg) requires additional computations to explore the dynamics thoroughly.

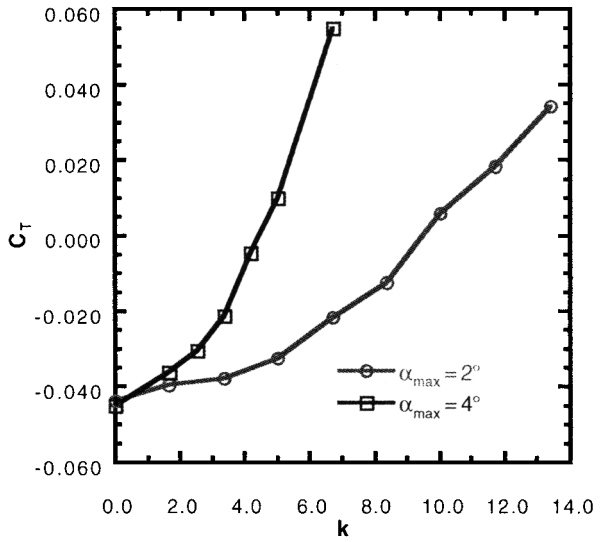

a) C_T vs reduced frequency

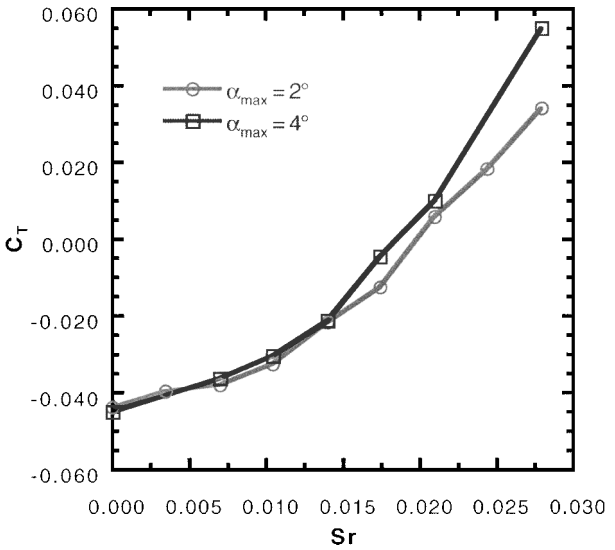

b) C_T vs Strouhal number

Fig. 5 Variation of thrust coefficient for $Re = 1.2 \times 10^4$.

Pitching and Heaving Airfoil

Katz and Weihs[17] have studied large-amplitude motions of a hydrofoil, both pitching and heaving motions, with chordwise flexibility to study propulsion in fishes. They found that the thrust increases with increasing frequency, amplitude of motion, and angle

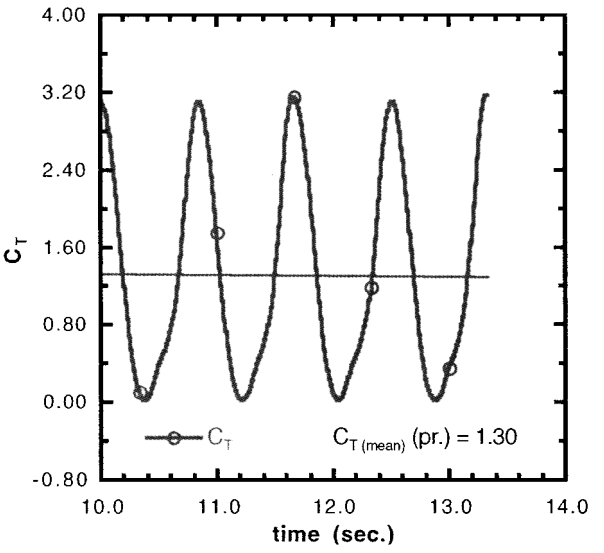

a) Pressure component

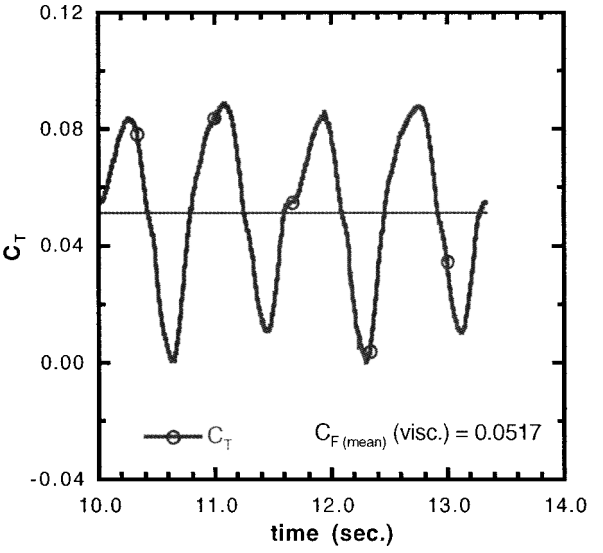

b) Viscous component

Fig. 6 Variation of thrust coefficient for a pitching and heaving NACA 0012 airfoil.

of attack. They observed that the highest thrust and efficiency occurs when the heave motion lags the pitching motion by approximately 90 deg. Isogai et al.[18] have studied the effects of dynamic stall on the thrust of pitching and heaving airfoils at $Re = 10^5$. Anderson[2] has experimentally studied the pitching and heaving motion of a NACA0012 airfoil for an array of frequencies and amplitudes of the heaving motion and phasing between the two motions. She has studied the effect of the leading-edge separation on the wake structure, the effect of the Strouhal number on the thrust and vortex strength, and the influence of the phase angle on the dynamic stall vortices and, hence, the thrust generation. In the present study, we have selected some of the cases from Anderson's work and compared our computational results with the experimental data.

The first case that was selected was of a pitching and heaving NACA0012 airfoil at $Re = 1.1 \times 10^3$, based on the chord of the airfoil, with the heaving motion lagging the pitching motion by 90 deg. The nondimensional frequency, $f^* = fc/2U_\infty$ selected was 0.3, the pitch amplitude $\theta_0 = 15$ deg, and the heave amplitude $A = c$. This translates to a Strouhal number bases on chord $Sr_c = 0.6$. The simulation was carried out for eight cycles of oscillation using a grid consisting of 23,331 points and 46,274 triangles. The variation of the force coefficient due to the pressure and viscous components with time are shown in Fig. 6. The total mean thrust coefficient is 1.35. The thrust coefficient from Ref. 2 for this case is 1.2.

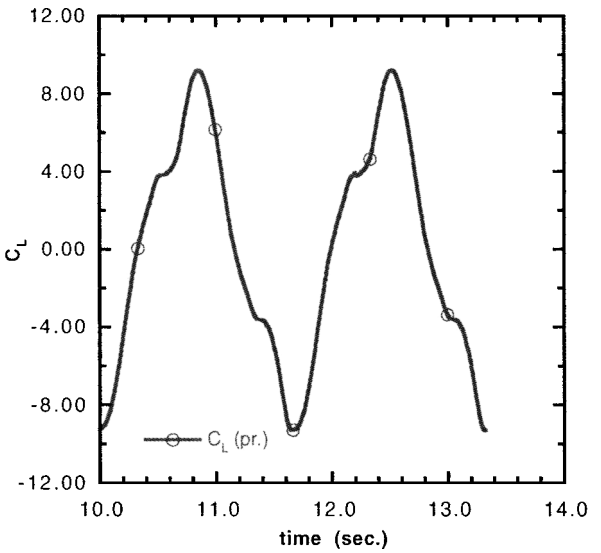

Fig. 7 Variation of lift coefficient for a pitching and heaving airfoil, $\phi = 90$ deg and $f^* = 0.3$.

The variation of lift coefficient for this case is shown in Fig. 7. A harmonic analysis of the variation of the lift coefficient with time shows that the first harmonic lags the prescribed heaving motion, Eq. (11), by 98 deg. Also, Fig. 7 shows that there is a narrow period, between $t = 10.5$ and 10.6 s, during which the lift is almost constant. A closer examination of the vorticity distributions shows that a vortex with a positive sign is attached on the top surface of the airfoil (Figs. 8a–8c) and is lifted off the surface (Fig. 8d) when the lift begins to recover.

Next, simulations were performed for several phase angles ϕ ranging from 30 to 140 deg and for $f^* = 0.45$. The pitch amplitude in this case was 30 deg, and the heave amplitude was retained to be equal to the chord. From Fig. 9a, it can be seen that the coefficient of force reaches a maximum at a $\phi = 120$ deg. The comparison with the experiments of Anderson[2] is good except for the $\phi = 90$ deg data point. The experimental data show that there is a drop in C_T at $\phi = 100$ deg, and a subsequent increase at $\phi = 110$ deg. We see no physically compelling reason for this trend. Isogai et al.[18] have shown that for higher reduced frequencies, the maximum thrust occurs at $\phi = 120$ deg rather that at 90 deg. In Fig. 9b, the variation of the lift coefficient component due to pressure, C_{lp}, that due to the viscous forces, C_{lv}, and the total C_l with the phase angle are shown. The lift coefficient achieves a maximum at $\phi = 50$ deg, drops to a negative value at $\phi = 120$ deg and then increases to a positive value at $\phi = 140$ deg. Note that the phase angle for the maximum force, $\phi = 120$ deg, is not desirable for lift generation. For example, if the required lift coefficient to balance the weight and any vertical acceleration is 0.02, then the optimal ϕ would be 100 deg; if the required lift coefficient is 0.09, then the optimal ϕ would be 50 deg. The propulsive efficiency for this case is computed as follows:

$$\eta = TU_\infty / P \tag{16}$$

where P is the power input. This reduces in nondimensional terms to

$$\eta = C_T / C_p \tag{17}$$

where

$$C_p = -(C_l \dot{y} + C_m \dot{\theta}) \tag{18}$$

Figure 10 shows that the propulsive efficiency achieves a maximum of approximately 0.3 at around $\phi = 90$ deg. Similar results

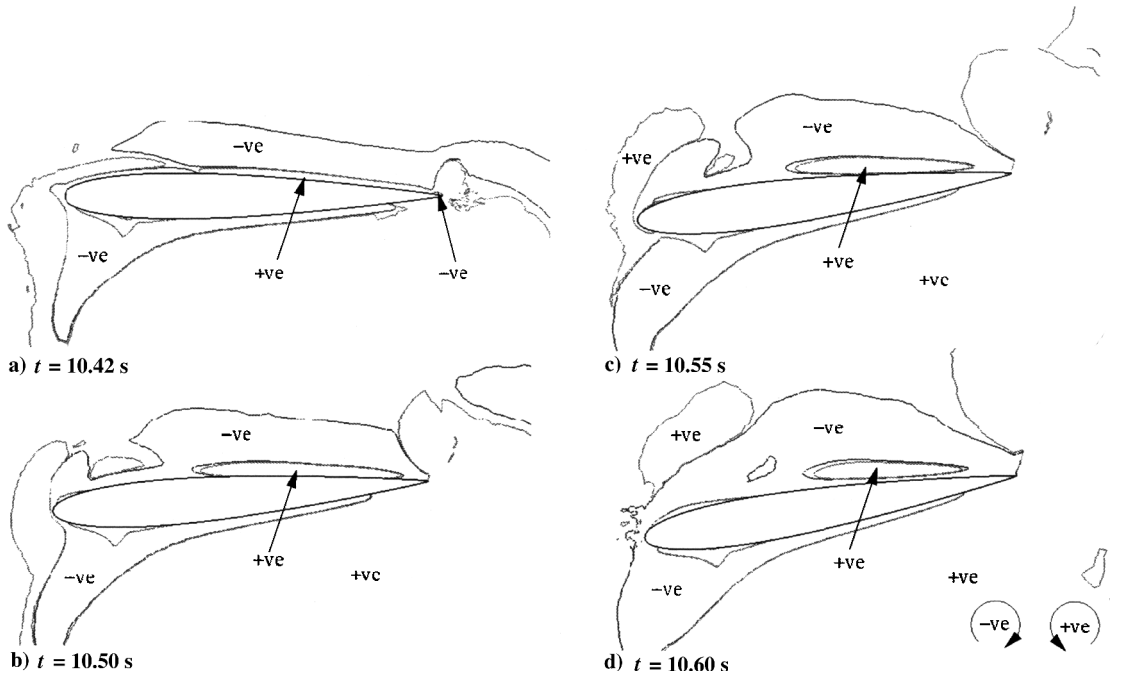

Fig. 8 Vorticity contours for a pitching and heaving airfoil, $Re = 1.1 \times 10^3$ and $f^* = 0.3$.

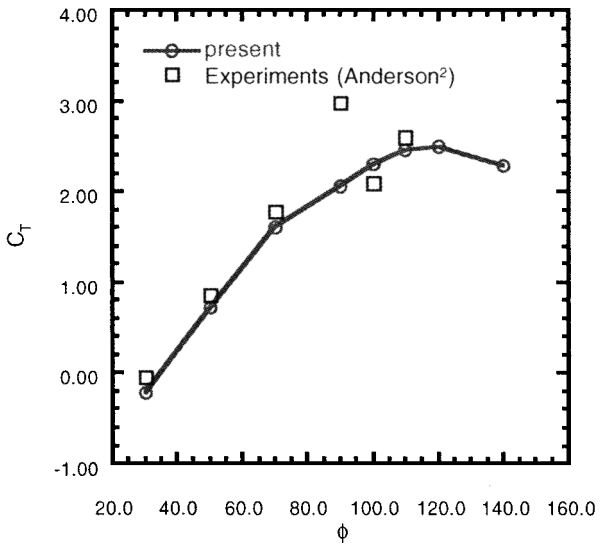

a) Thrust coefficient

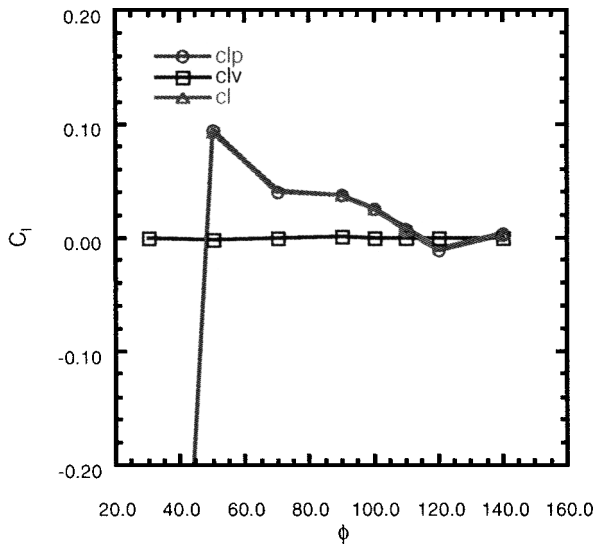

b) Lift coefficient

Fig. 9 Variation of thrust and lift coefficients for a pitching and heaving airfoil; $Re = 1.1 \times 10^3$ and $f^* = 0.45$.

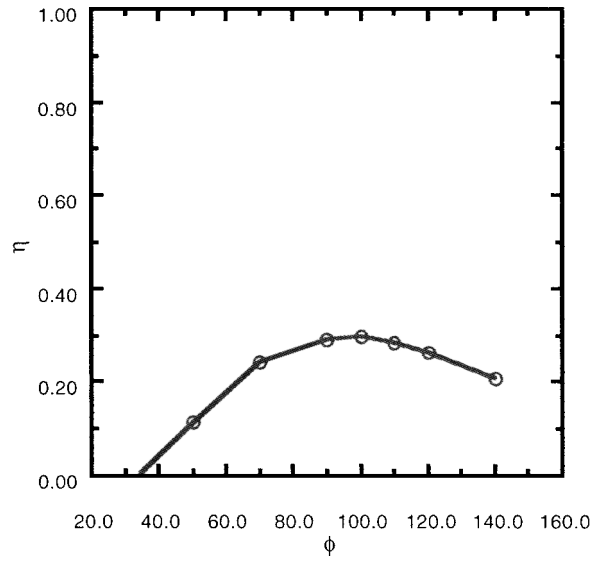

Fig. 10 Variation of propulsive efficiency with phase angle; $f^* = 0.45$ and $Re = 1.1 \times 10^3$.

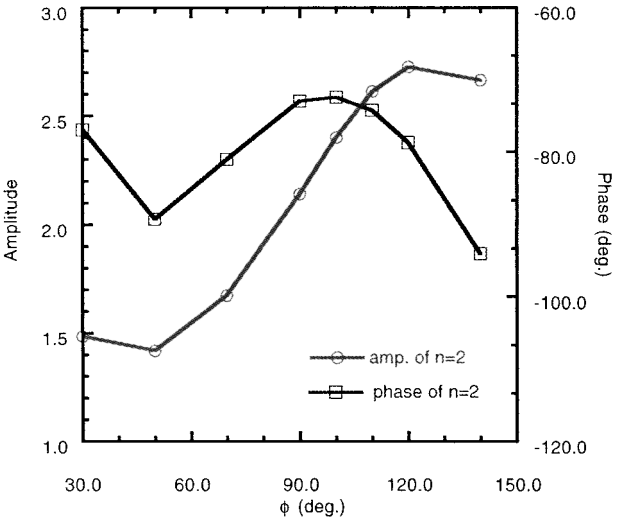

a) Thrust coefficient

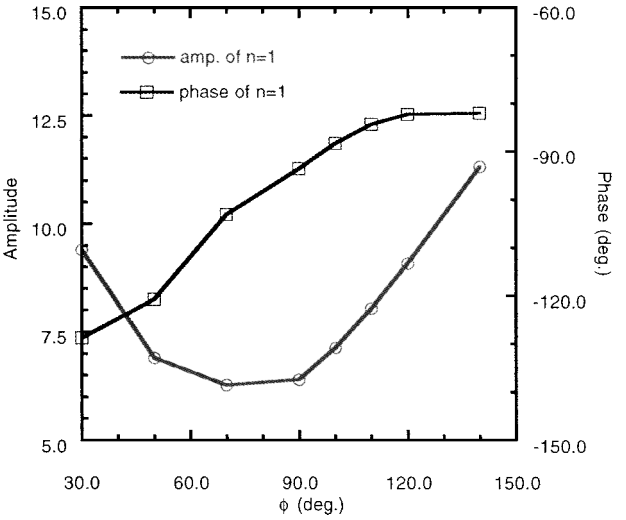

b) Lift coefficient

Fig. 11 Variation of the amplitude and phase of the harmonics of the thrust and lift coefficients.

were obtained by Isogai et al.[18] A harmonic analysis of the last two cycles of simulation was performed for all of these cases. The amplitude and phase shift from the heaving motion of the second harmonic in the time variation of the force coefficient and the first harmonic in the time variation of the lift coefficient are shown in Figs. 11a and 11b, respectively. In Fig. 11a, the amplitude of the second harmonic, $n = 2$, of C_T reaches a minimum at $\phi = 50$ deg, although the mean thrust coefficient at this phase angle is higher than that at $\phi = 30$ deg, and it reaches a maximum at $\phi = 120$ deg. From Fig. 11b, the amplitude reaches a minimum at $\phi = 70$ deg, although the mean lift coefficient attains a minimum at $\phi = 120$ deg. The phase shift for the lift coefficient increases with increase in the phase angle between the pitch and heave motions.

Summary

A finite element flow solver based on unstructured grids was employed to compute unsteady flow past a NACA0012 airfoil undergoing both pitching as well as pitching and heaving motions. A grid refinement study was performed for the case of a pitching airfoil, and grid independent solution for the thrust coefficient was achieved. The variation of the thrust coefficient with reduced frequency was compared to experimental studies of Koochesfahani[1] and numerical studies of Jones and Platzer.[3] To address the differences between the current study and the experiments, a wake analysis and computations with tunnel walls were performed. In both of these cases, the force coefficient obtained from the integration of wake velocity

agreed with that obtained from the integration of surface pressure and shear on the airfoil. The differences between the experimental data and the computations are due to the exclusion of a contribution of the fluctuating quantities and pressure term in the experimental thrust computation at the measuring location.

The effect of variation of the amplitude of pitching motion on the thrust coefficient showed that the critical parameter for thrust generation is not the reduced frequency, but rather the Strouhal number based on the wake width or the trailing-edge displacement.

For the case of the pitching and heaving airfoil, several computations were performed, varying the phase angle between the two motions. Good agreement was obtained with the experimental results of Anderson.[2] A close examination of the time variation of the lift coefficient showed that a slight loss in lift during the cycle was due to a vortex attached to the top surface of the airfoil. When this vortex lifted off of the surface, the lift force began to recover. Thus, the ability of the code to identify the transients in lift signatures of the passage of well-identified vortices over the airfoil surface has been demonstrated. It has also been shown that the thrust coefficient attains a maximum value when the pitching motion leads the heaving motion by 120 deg, and the maximum propulsive efficiency is achieved when the phase difference is 90 deg.

Acknowledgments

This work was supported by the Office of Naval Research through the Tactical Electronic Warfare Division of the Naval Research Laboratory (NRL). The authors would like to thank Rainald Löhner of George Mason University and Kevin Ailinger of NRL for their assistance and support throughout the course of this work.

References

[1]Koochesfahani, M., "Vortical Patterns in the Wake of an Oscillating Airfoil," *AIAA Journal*, Vol. 27, No. 9, 1989, pp. 1200–1205.

[2]Anderson, J. M., "Vorticity Control for Efficient Propulsion," Ph.D. Dissertation, Applied Ocean Science and Engineering, Massachusetts Inst. of Technology, Cambridge, MA, Feb. 1996.

[3]Jones, K. D., and Platzer, M. F., "Numerical Computation of Flapping-Wing Propulsion and Power Extraction," AIAA Paper 97-0826, Jan. 1997.

[4]Tuncer, I. H., and Platzer, M. F., "Thrust Generation Due to Airfoil Flapping," *AIAA Journal*, Vol. 34, No. 2, 1996, pp. 324–331.

[5]Ramamurti, R., Sandberg, W. C., and Löhner, R., "Simulation of a Torpedo Launch Using a Three-Dimensional Incompressible Finite Element Flow Solver and Adaptive Remeshing," AIAA Paper 95-0086, Jan. 1995.

[6]Martin, D., and Löhner, R., "Implicit Linelet-Based Solver for Incompressible Flows," AIAA Paper 92-0668, 1992.

[7]Ramamurti, R., and Löhner, R., "Evaluation of an Incompressible Flow Solver Based on Simple Elements," *Advances in Finite Element Analysis in Fluid Dynamics*, FED Vol. 137, edited by M. N. Dhaubhadel, M. S. Engelman, and J. N. Reddy, American Society of Mechanical Engineers, New York, 1992, pp. 33–42.

[8]Ramamurti, R., Löhner, R., and Sandberg, W. C., "Evaluation of Scalable Three-Dimensional Incompressible Finite Element Solver," AIAA Paper 94-0756, 1994.

[9]Meirovitch, L., *Methods of Analytical Dynamics*, McGraw–Hill, New York, 1970, pp. 122–143.

[10]Sandberg, W. C., "The Estimation of Ship Motion Induced Loads," *Proceedings of the 4th Ship Technology and Research Symposium*, Society of Naval Architects and Marine Engineers, Atlanta, GA, 1979, pp. 347–351.

[11]Löhner, R., "An Adaptive Finite Element Solver Transient Problems with Moving Bodies," *Computers and Structures*, Vol. 30, No. 1, 1988, pp. 303–317.

[12]Löhner, R., and Baum, J. D., "Three-Dimensional Store Using a Finite Element Solver and Adaptive Remeshing," AIAA Paper 91-0602, 1991.

[13]Boschitsch, A. H., and Quackenbush, T. R., "High-Accuracy Computations of Fluid–Structure Interaction in Transonic Cascades," AIAA Paper 93-0485, 1993.

[14]Batina, J. T., "Unsteady Euler Airfoil Solutions Using Unstructured Dynamic Meshes," *AIAA Journal*, Vol. 28, No. 8, 1990, pp. 1381–1388.

[15]Rausch, R. D., Batina, J. T., and Yang, H. T. Y., "Three-Dimensional Time Marching Aeroelastic Analysis Using an Unstructured Grid Euler Method," *AIAA Journal*, Vol. 31, No. 9, 1993, pp. 1626–1633.

[16]Liu, H., and Kawachi, K., "A Numerical Study of Undulatory Swimming," *Journal of Computational Physics*, Vol. 155, No. 2, 1999, pp. 223–247.

[17]Katz, J., and Weihs, D., "Hydrodynamic Propulsion by Large Amplitude Oscillation of an Airfoil with Chordwise Flexibility," *Journal of Fluid Mechanics*, Vol. 88, No. 3, 1978, pp. 485–497.

[18]Isogai, K., Shinmoto, Y., and Watanabe, Y., "Effects of Dynamic Stall on Propulsive Efficiency and Thrust of Flapping Foil," *AIAA Journal*, Vol. 37, No. 10, 1999, pp. 1145–1151.

P. R. Bandyopadhyay
Associate Editor